

Article

# Rolling Contact Performance of a Ti-Containing MoS<sub>2</sub> Coating Operating Under Ambient, Vacuum, and Oil-Lubricated Conditions

Harpal Singh <sup>1,2,\*</sup>, Kalyan C. Mutyala <sup>1,3,†</sup>  and Gary L. Doll <sup>1</sup>

<sup>1</sup> Timken Engineered Surfaces Laboratories, The University of Akron, Akron, OH 44325, USA; km107@zips.uakron.edu (K.C.M.); gd27@uakron.edu (G.L.D.)

<sup>2</sup> Sentient Science, West Lafayette, IN 47906, USA

<sup>3</sup> Ford Motor Company, Dearborn, MI 48124, USA

\* Correspondence: hs53@zips.uakron.edu

† Authors contributed equally.

Received: 22 October 2019; Accepted: 9 November 2019; Published: 13 November 2019



**Abstract:** Solid lubricant molybdenum disulfide (MoS<sub>2</sub>) coatings have been frequently used to lubricate mechanisms operating in environments where oil and grease lubrication are ineffective. This work evaluated the rolling contact performance of a Titanium-containing MoS<sub>2</sub> coating under humid ambient, vacuum, and oil-lubricated conditions. Weibull analyses of L<sub>50</sub> lifetimes of AISI 52100 steel balls coated with a Ti-MoS<sub>2</sub> coating paired with uncoated M50 steel rods were determined to be 3.7, 14.5, and 158.6 million cycles in ambient, vacuum, and oil-lubricated environments, respectively. In the ambient and vacuum tests, failures were determined to be associated with the onset of abrasive wear rather than fatigue or spalling. The L<sub>50</sub> lifetimes of tests performed in those environments were found to depend upon the wear rate of the coatings on the balls. That is, the Ti-MoS<sub>2</sub> functioned as a barrier to the onset of abrasive wear between the steel alloys until the coating was sufficiently worn away. Under oil-lubricated (boundary lubrication) conditions, L<sub>50</sub> was found to depend on the durability and composition of tribofilms formed in-situ on the surfaces of the uncoated M50 rods. The tribofilms were comprised of mixtures of MoS<sub>2</sub> crystallites and amorphous hydrocarbon (a-C:H). The crystalline MoS<sub>2</sub> in the tribofilm originated from the amorphous Ti-MoS<sub>2</sub> coating and likely underwent a thermodynamic phase transition as a result of the applied Hertz stress and frictional heating in the contact. The a-C:H in the tribofilm probably originated from a catalytic scission of the polyalphaolefin (PAO) molecules caused by the d-band character of the Mo or Ti in the coating. Overall, the Ti-MoS<sub>2</sub>-coated balls were effective at extending the operational lifetimes of M50 rods under ambient, vacuum, and oil-lubricated conditions by an order of magnitude.

**Keywords:** MoS<sub>2</sub>; solid lubricant; transfer layer; aerospace/space; velocity accommodation layer

## 1. Introduction

Holmberg and Erdemir estimated that about 23% of global energy is consumed to overcome friction and associated wear losses [1]. Whereas oil and grease lubrication are used to minimize friction and wear losses in most situations, in challenging environments such as high vacuum, solid lubricants such as molybdenum disulfide (MoS<sub>2</sub>) are often employed [2]. Numerous studies established that interfilm sliding and intrafilm flow control the lubricity and the durability of MoS<sub>2</sub>. The primary reason for its ability to reduce friction has been attributed to its crystal structure (D<sub>4h</sub><sup>6</sup>-P6<sub>3</sub>/mmc) with strong in-plane and weak out-of-plane bonding, which allows easy shearing of the MoS<sub>2</sub> layers. MoS<sub>2</sub> crystallites in coatings were also observed to have a tendency to reorient from an initially random orientation to a state where the (002) basal planes were parallel to the surface [3,4]. MoS<sub>2</sub> based

coatings are used as solid lubricants in aerospace/space applications such as actuators and slip rings, among many others [5–7]. In ambient conditions, the tribological performance of MoS<sub>2</sub> degrades in the presence of moisture and oxygen due to reactions occurring with edge sites of crystallites that inhibit basal plane shearing and thereby increase the friction coefficient and wear rate [8,9].

To improve the tribological performance of MoS<sub>2</sub> in ambient conditions, researchers developed various technologies that can be broadly classified into two categories. In the first category, oxidation was minimized and improved tribological, structural, and mechanical properties were obtained by doping MoS<sub>2</sub> coatings with metals (Ti, Cr, Zr, Au, Pb, Ni), oxides (Sb<sub>x</sub>O<sub>y</sub>, Pb<sub>x</sub>O<sub>y</sub>), and other nanomaterials [10–16]. In the second category, MoS<sub>2</sub> in various forms, such as bulk powder and nanosized particles, have been employed as additives to work synergistically with oil-based lubricants [17–21]. Previous studies [6,22] have shown that MoS<sub>2</sub> coatings doped with Titanium had vastly improved tribological performance and mechanical properties to sputter-deposited, undoped MoS<sub>2</sub> coatings. The improvement in mechanical properties, load bearing capacity, and wear resistance over pure MoS<sub>2</sub> has been attributed to the dopant content [23–25]. Although the friction and wear performance of the doped MoS<sub>2</sub> coatings have been well-studied in unidirectional and reciprocating sliding contact, limited studies have been conducted on these coatings under rolling or mixed mode contact. The first rolling contact studies involving a Ti-doped MoS<sub>2</sub> coating were previously published in [22,24]. The goal of this work was to achieve a better understanding of the science behind the rolling contact performance of Ti-MoS<sub>2</sub>-coated balls by comparing test results conducted in ambient, vacuum, and boundary-lubricated environments.

## 2. Materials and Methods

### 2.1. Deposition

Ti-doped MoS<sub>2</sub> composite coatings were deposited onto bearing grade AISI 52100 steel balls (12.5 mm diameter; average surface roughness  $R_a$ : 0.015  $\mu\text{m}$ ) and AISI 52100 steel disk specimens ( $R_a$ : 0.2  $\mu\text{m}$ ). Specimens were ultrasonically cleaned in an alkaline detergent, rinsed in deionized (DI) water, and dried before mounting on fixtures in a custom built closed-field unbalanced magnetron sputtering system (CFUMS). The deposition chamber was evacuated to a pressure of  $1 \times 10^{-5}$  Torr and substrates were plasma-etched at a bias voltage of  $-500$  V in an Argon partial pressure of  $1.6 \times 10^{-3}$  Torr. Two MoS<sub>2</sub> and two Ti targets were sputtered with currents of 1.3 A and 0.6 A, respectively. The coatings were deposited with an Ar (purity 99.9%) gas flow maintained at 50 sccm and substrate temperature of less than 80 °C. AISI 52100 balls were mounted on small magnets during the deposition process and were rotated independently on the ball axis, as well as the fixture table axis, during the deposition.

### 2.2. Characterization

Coating thickness was measured nondestructively by X-ray fluorescence (XRF, Fischerscope, Sindelfingen, Germany) and was uniform on the balls—except for the uncoated spots that were in contact with the magnets during the deposition. The elemental composition of the films was measured by X-ray energy dispersive spectroscopy (XEDS, EDAX Inc, Mahwah, NJ, USA). Adhesion between the coating/substrate interface was evaluated using an HRC Rockwell diamond indenter according to Verein Deutscher Ingenieure (VDI) guidelines [26]. Raman spectroscopy was performed on various locations on the coated specimens using a Micro-Raman spectrometer (Horiba, Kyoto, Japan) with an excitation wavelength of 532 nm and a 50 $\times$  objective. Focused ion beam scanning electron microscopes (Nova 200, FEI, Hillsboro, Oregon and Lyra 3, Tescan, Kohoutovice, Czech Republic) were used to examine the coating architecture in cross-section on disk and ball specimens.

### 2.3. Tribological Test Apparatus and Procedure

Rolling contact fatigue (RCF) performance of Ti-MoS<sub>2</sub>-coated AISI 52100 [27] balls and uncoated M50 rods were studied under vacuum conditions in a custom-built Vacuum RCF (V-RCF) tester

(Figure 1). The design of the rolling contact fatigue test head assembly was adapted from a three-ball-on-rod test rig developed by Glover [28]. The V-RCF tribometer was equipped with vibration (accelerometer) and temperature sensors, as well as data acquisition capabilities (Figure 1c). The vibration sensor was programmed to terminate the test in the event of excessive vibration (set limit: 4G) corresponding to either a ball or rod spall, or excessive wear. The tester was constructed with a top-down assembly approach (Figure 1a) and mechanical springs were used to apply radial loads (Figure 1b).

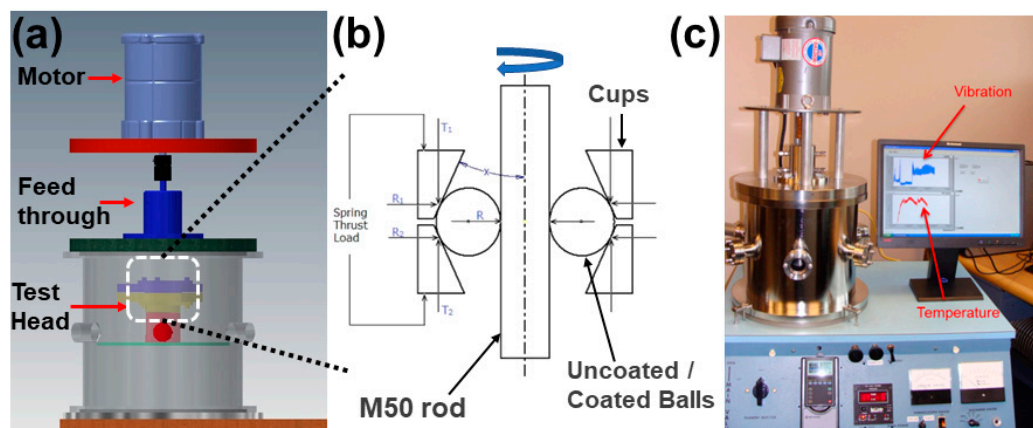


**Figure 1.** Designed vacuum rolling contact (V-RCF) tester: (a) Computer Aided Design (CAD) assembly of the designed V-RCF; (b) schematic showing rod, cups and ball configuration, along with radial loads; (c) as-built V-RCF with data acquisition capabilities.

A brass ball retainer is typically used in conventional three-ball-on-rod test rigs to maintain separation of the balls around the circumference of the rod. However, in baseline testing performed under vacuum in the V-RCF tribometer, it was discovered that brass from the retainer was transferred to the rod and balls and behaved as a solid lubricant. Therefore, a full complement of five balls was used in the V-RCF test rig to eliminate the tribological and vibrational contributions arising from the ball holder [29,30]. Axial loads applied to the cups produced radial loads on the rods (Figure 1b), yielding a contact stress of  $\sim 1$  GPa in the five-ball configuration. Springs were calibrated prior to each test to minimize variations in the applied load. These tests were conducted in both vacuum and ambient (40–45% RH) atmospheres at rotational speeds of 3450 rpm and at 3600 rpm, respectively. V-RCF tests began after the chamber pressure reached  $1 \times 10^{-5}$  Torr and tests were terminated when vibration exceeded the 4G value measured by the accelerometer.

RCF performance of the Ti-MoS<sub>2</sub> coating under boundary lubrication conditions (drip-fed PAO ISO 10 oil at 4–5 drops/min—estimated lambda ( $\lambda$ ) [31] value between 0.1 and 0.3) was conducted on a conventional three ball-on-rod tribometer at a contact stress of 5.0 GPa. Since balls do not precess in ball-on-rod tribometers, the balls were oriented in the assemblies such that their uncoated spots did not come into contact with the M50 rods or cups. Baseline experiments were recorded with uncoated rods (M50) and uncoated balls (AISI 52100) in ambient, vacuum, and boundary-lubricated conditions. Experiments were then conducted by replacing the uncoated AISI 52100 balls with Ti-MoS<sub>2</sub>-coated balls and testing new M50 rods under the same conditions as the baseline tests. A minimum of three datapoints were obtained for each material combination in all three test environments. In each test, a new location on a M50 rod was used, along with a new set of balls. The accelerometer cutoff value for this experiment was set to 10G. Weibull analysis was performed using a least square estimate method to estimate the operational lifetimes ( $L_{10}$  and  $L_{50}$ ) of the material combinations under ambient, vacuum, and boundary-lubricated conditions.

### 3. Results and Discussion

#### 3.1. Characterization

Cross-sectional TEM and SEM images in Figure 2a,b display the architecture of the Ti-MoS<sub>2</sub> coating. Specifically, the coating consisted of a ~200 nm Ti bond layer, a ~150 nm compositionally graded layer of Ti and MoS<sub>2</sub>, and a ~650 nm top layer of Ti-MoS<sub>2</sub>. The total thickness of the coating was ~1 μm and its adhesion to the disk samples was rated excellent (HF-1) based on the VDI guidelines. The microstructural morphology of the coating was columnar on both disk (Figure 2a) and ball (Figure 2b) substrates, although the columns in the coating on the ball were larger and less dense than the columns in the coating on the disk specimen. Although the balls (thickness: 850 nm) and disks (thickness: 1000 nm) were coated in the same deposition run, the balls underwent three-axis rotation, while the disks were mounted such that they faced the sputter targets and experienced two-axis rotation during the deposition. It is believed that the different morphologies produced on the disks and balls can be attributed to the interaction of the flux of the sputtered material with the geometry of the substrates (flat vs sphere) [32–34] as well as the substrate rotation mode (two-axis vs. three-axis).

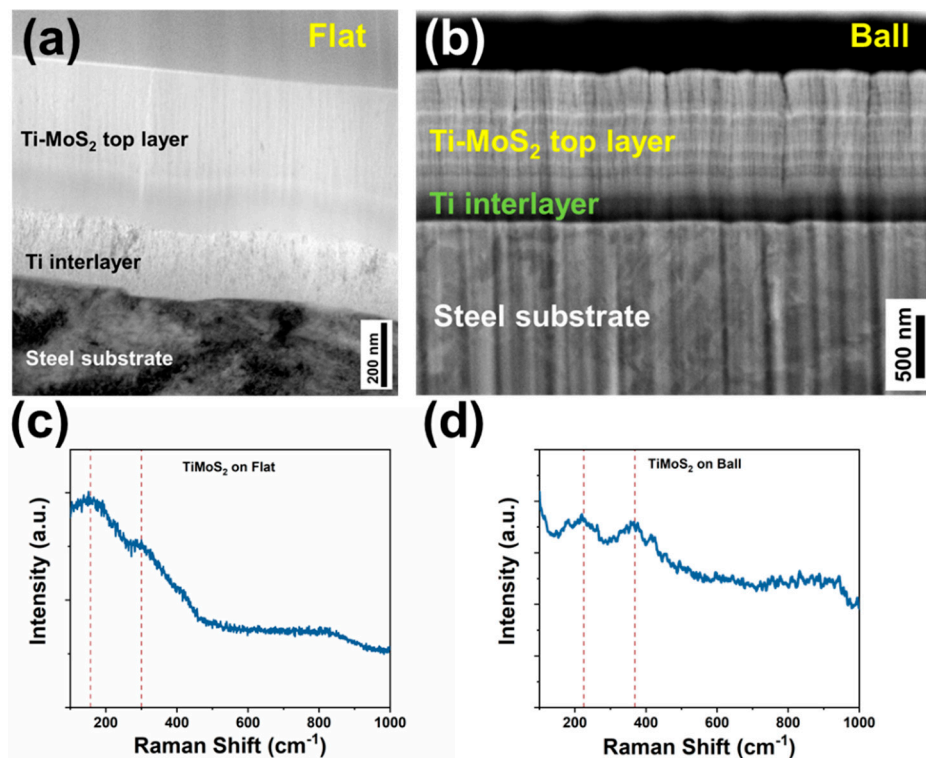


**Figure 2.** Ti-MoS<sub>2</sub> coating cross-sectional: (a) TEM image on a flat (disc) sample; (b) SEM image on a ball sample; (c,d) Raman spectra of untested Ti-MoS<sub>2</sub> from the flat and ball specimens.

The elemental composition of the coating was ascertained with X-ray energy dispersive spectroscopy (XEDS) to obtain an approximate at % of the constituent elements. Coatings on both disks and balls were found to contain about 16 at % Ti and had a S/Mo ratio of 1.8. The significant overlap between S and Mo peaks in XEDS rendered the measured stoichiometric ratio (1.8) as approximate. Raman spectra of the as-deposited Ti-MoS<sub>2</sub> on disk and ball specimens are shown in Figure 2c,d. The spectra are typical of a material possessing little or no crystallinity. The two broad, low-wavenumber features were attributed to vibrations arising from amorphous MoS<sub>2</sub>. Inclusion of Ti in the MoS<sub>2</sub> is known to inhibit the ability of the MoS<sub>2</sub> to crystallize during deposition, to reduce coating porosity, increase coating density, and produce better mechanical properties compared to undoped MoS<sub>2</sub> coatings [10,11,35]. Interestingly, whereas the peaks reside at ~150 and ~300 cm<sup>-1</sup> in

the Raman spectrum of the coating on the disk, the features fall at  $\sim 220$  and  $360\text{ cm}^{-1}$  in the spectrum of the coating on the ball. This observation indicates that there are subtle differences in the bonding associated with the vibrations giving rise to these photons between the coatings on the disk and ball.

In previously published studies of Ti-MoS<sub>2</sub> deposited with the same recipe as the coatings in this work, we examined the microstructure and investigated the position and distribution of Ti in the Ti-MoS<sub>2</sub> layer [22,25]. High-resolution transmission electron microscopy (HRTEM) results included in those studies clearly showed the amorphous (incoherent) nature of the Ti-MoS<sub>2</sub> top layer and a random crystalline orientation of the Ti adhesion layer. That is, it was observed that no crystalline order was detected at the nanometer scale in the Ti-MoS<sub>2</sub> layer. The homogeneous distribution of the elements in Ti-MoS<sub>2</sub> layer was confirmed by atom probe tomography (APT) analysis published in a separate study [25]. A reconstruction of the Ti-MoS<sub>2</sub> top layer revealed that the Ti, Mo, and S atoms were homogeneously dispersed with no sign of clusters or precipitates. The APT results were consistent with complementary electron diffraction results from these coatings.

### 3.2. Tribological (RCF) Performance

Operational lives are typically estimated using Weibull analysis [36]. A Weibull distribution is a continuous probability distribution that is drawn on a double logarithm diagram based on the individual failures. The graphical representation of failures is fitted with a Weibull line, which reveals information about the shape (slope,  $\beta$ ) and scale ( $\eta$ ) parameters that correspond to the characteristic life (life at which 63.2% of a population will fail or 36.8% will survive) and failure rate of the specimen. Weibull analysis results of coated and uncoated material pairs tested in ambient, vacuum, and oil-lubricated environments are shown in Figure 3a–c, respectively. Weibull parameters can be determined using different methods, but the most common are median rank regression (MRR) and maximum likelihood estimation (MLE). MLE is more suitable for larger data sets, since the Weibull parameters can be overestimated with sample sizes of  $<10$ . Therefore, the Weibull parameters in this study were calculated using the MRR method (linear regression least-squares fit) due to its suitability for a smaller dataset [37]. The numerical analysis and Weibull parameters of tests performed in ambient air (RH 40–45%), vacuum, and oil-lubricated conditions are gathered in Table 1.

In all cases, the L<sub>10</sub> and L<sub>50</sub> lives (in millions of revolutions) of coated balls in all test conditions were higher than those of the baseline tests. L<sub>10</sub> and L<sub>50</sub> represent the life at a failure probability of 10% and 50%, regardless of the cause of failure. In the vacuum and ambient environments, the operational lifetimes of coated balls paired with uncoated rods were more than an order of magnitude greater than those of uncoated balls and rods. However, the lives of coated balls and uncoated balls in vacuum were significantly greater than the lives of coated and uncoated balls in ambient conditions. Although this result was anticipated for the tests performed with the Ti-MoS<sub>2</sub> coating present (due to the detrimental effect that water vapor has on the tribological performance of MoS<sub>2</sub>), the result for the tests performed with the uncoated specimens was unanticipated. Inspection of the rods and balls that were tested in the V-RCF under ambient and vacuum conditions revealed that the failure mode was wear and not fatigue. That is, spalls on the rods or balls were not observed. Reconciliation of the later observation may point to the roles that oxygen and moisture play in steel on steel rolling contact. That is, the ambient test results hint that chemical as well as mechanical interactions may have played a role in the failure mechanism of the M50 rods and uncoated AISI 52100 balls. In other words, the presence of oxygen and/or moisture accelerated the abrasive wear mechanism associated with the steel on steel contact.

The Ti-MoS<sub>2</sub> coating on the balls was found to improve the L<sub>50</sub> life over that of the tests with the uncoated balls in the oil-lubricated environment. In the oil-lubricated environment, it was apparent that the Ti-MoS<sub>2</sub> coating on the balls did not function as a solid lubricant, but as an additive source. The significant increase in the life of the M50 rods when paired with Ti-MoS<sub>2</sub>-coated balls suggests synergistic interactions between the oil and the Ti-MoS<sub>2</sub> coating. Inspection of the rods and balls tested in the oil-lubricated environment revealed that the source of failure was, in all cases, the generation of a spall on the M50 rods. Additionally, black bands were found in the wear tracks created on the

M50 rods. Overall, the Ti-MoS<sub>2</sub>-coated balls were effective at extending the operational lifetimes of M50 rods under ambient, vacuum, and oil lubricated conditions by an order of magnitude. All tests conducted with Ti-MoS<sub>2</sub>-coated balls lasted a significantly higher number of cycles compared to uncoated specimens in vacuum, ambient, and oil-lubricated conditions. The comparison of L<sub>50</sub> lives of uncoated (red) and coated (blue) pairs in different operating conditions is shown in Figure 3d. The blocks represent 65% confidence limits and L<sub>50</sub> life is shown by the centerline. A clear difference is seen in the life of coated balls and uncoated pairs, where Ti-MoS<sub>2</sub> coating significantly improved life material pairs in three environments.

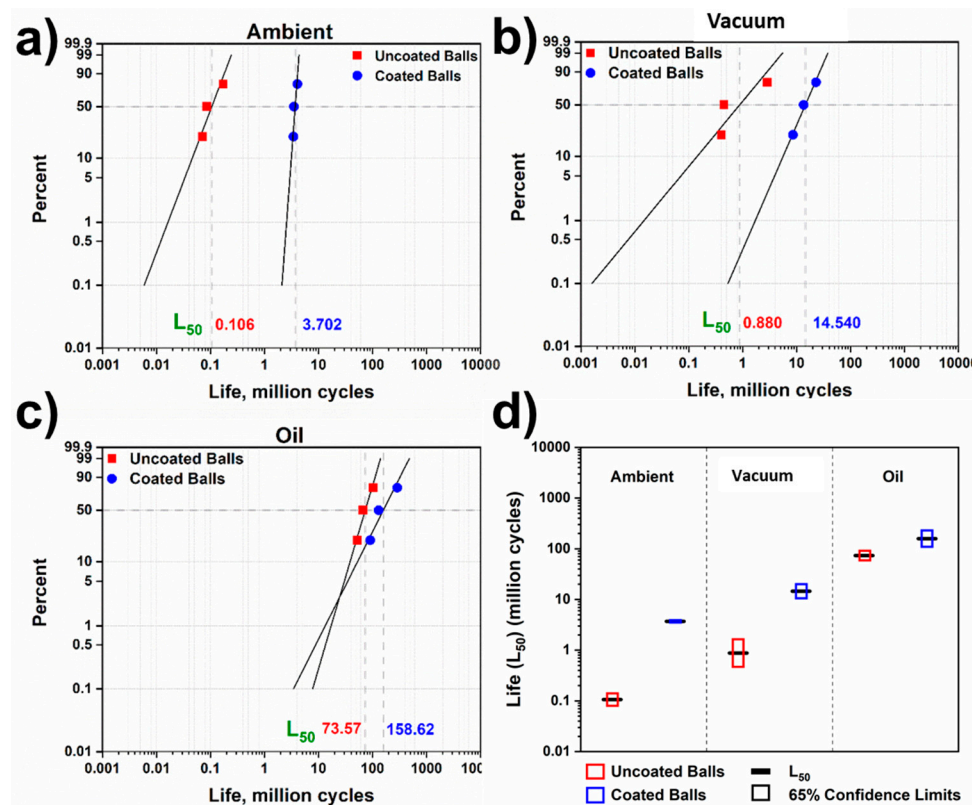


**Figure 3.** Weibull analysis of failure data for the material pairs tested under (a) ambient (RH 40–45% RH), (b) vacuum, and (c) oil-lubricated conditions. (d) Summary of L<sub>50</sub> life values with 65% confidence limits. Failures that occurred in the ambient and vacuum testing were caused by the onset of abrasive wear between the steel alloys. Failures that occurred in the oil-lubricated tests were caused by fatigue spalling of the M50 rods.

**Table 1.** RCF Weibull statistics (L<sub>10</sub>, L<sub>50</sub> are in million cycles) of material pairs tested under ambient, vacuum, and oil conditions.

Operating Environment	Test Pair (M50 rod vs ...)	Slope ( $\beta$ )	L <sub>10</sub>	L <sub>50</sub>	L <sub>50</sub> /L <sub>50</sub> (uncoated)
Ambient	Uncoated Balls	2.27	0.05	0.11	1.00
	Coated Balls	11.68	3.15	3.70	34.91
Vacuum	Uncoated Balls	1.04	0.14	0.88	1.00
	Coated Balls	1.98	5.61	14.54	16.52
Oil	Uncoated Balls	2.91	38.51	73.57	1.00
	Coated Balls	1.71	52.69	158.62	2.16

Weibull slopes ( $\beta$ ) of the lines are particularly significant and provide an understanding of the statistics of the failures. Scatter in the fatigue data is inversely proportional to the Weibull slope: Lower values indicate a greater dispersion of failure, while higher values suggest deterministic or wear out failures.  $\beta$  values from the RCF tests were all greater than 1, which indicates “wear out” rather than infant mortality ( $\beta < 1$ ) or random ( $\beta = 1$ ) failures. Since values of  $\beta$  roughly scaled as the amount of Ti-MoS<sub>2</sub> exposed in the contact, it is evident that the “wear out” of the M50 rods in these cases was delayed by the presence of the coating. The higher slope of Ti-MoS<sub>2</sub> coated balls paired with uncoated M50 rods in the ambient environment suggests that rapid wear occurred in the tests. Small scatter in life indicates that once the first failure occurred, there is high likelihood for increased failures. This may suggest that the Ti-MoS<sub>2</sub> coating transferred to the M50 counter-face and formed a velocity accommodation layer (VAL), which rapidly wore away under the humid conditions.

Post-test analysis conducted using the 3D optical interferometer on the wear tracks created on the test rods during the ambient, vacuum, and oil-lubricated tests are shown in Figure 4a–c, respectively. Raman scattering experiments were also conducted on the wear tracks at the locations marked in an effort to identify the character of the material formed in the wear tracks on the rods. In the ambient and vacuum tests, the vibration limit correlated with the depletion of the Ti-MoS<sub>2</sub> coatings at the contact interface as opposed to the occurrence of ball or rod spall. The phenomena of coating depletion at the interface resulting in high vibration was previously reported by Danyluk and Dhingra for silver coatings tested against M50 rods [38]. Wear tracks created on the rods during the tests in the ambient environment (Figure 4a,d) were formed from wear of the M50 rod with no evidence of transferred material or tribofilm formation. However, it is interesting to note that in ambient conditions, Ti-MoS<sub>2</sub>-coated balls improved the L<sub>50</sub> life by almost 35 times (Table 1). Here, the mechanism can be attributed to the ability of Ti-MoS<sub>2</sub> to maintain a barrier to abrasive wear until the coatings on the balls were sufficiently worn away.

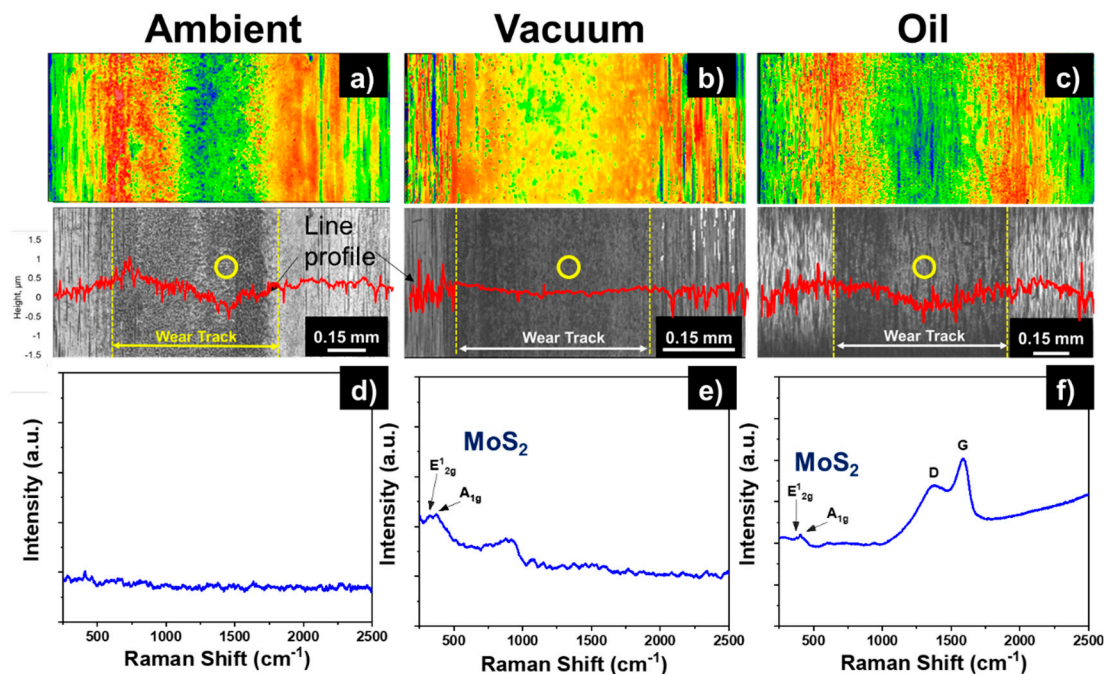


**Figure 4.** Post-test analyses of wear tracks generated on M50 rods. Three-dimensional optical interferometer images and line profiles from (a) ambient, (b) vacuum, and (c) oil-lubricated tests. Raman spectra (d–f) are shown for the three environments which were obtained from the locations marked by the yellow circles in the images.

Analyses of rods tested in the vacuum environment showed traces of MoS<sub>2</sub> material in the wear tracks (Figure 4b,e). The two broad peaks in the Raman spectrum were similar in shape to peaks

observed in the spectrum of the as-deposited (Figure 2d) amorphous structure of the Ti-MoS<sub>2</sub>, but also upshifted to a higher wavenumber. However, a closer inspection of the low wavenumber feature revealed that the superpositions of the two sharper peaks at 329 and 375 cm<sup>-1</sup> are consistent with frequencies of the E<sup>1</sup><sub>2g</sub> and A<sup>1</sup><sub>g</sub> phonons of crystalline MoS<sub>2</sub> [39]. Coated balls improved the L<sub>50</sub> life by ~16.5 times compared to the steel on steel baseline in tests conducted in vacuum. In vacuum conditions, the failure mechanism was similar to that which occurred in the ambient test, i.e., the Ti-MoS<sub>2</sub> coating on the balls delayed the onset of abrasive steel on steel wear until the coating was worn away. Due to reduced presence of moisture and oxygen, the MoS<sub>2</sub> that was transferred from the balls to the rods possessed a small amount of crystallinity in the otherwise amorphous film. A schematic representation of the mechanism responsible for the performance of Ti-MoS<sub>2</sub> coating in ambient, vacuum, and oil environments is shown in Figure 5.

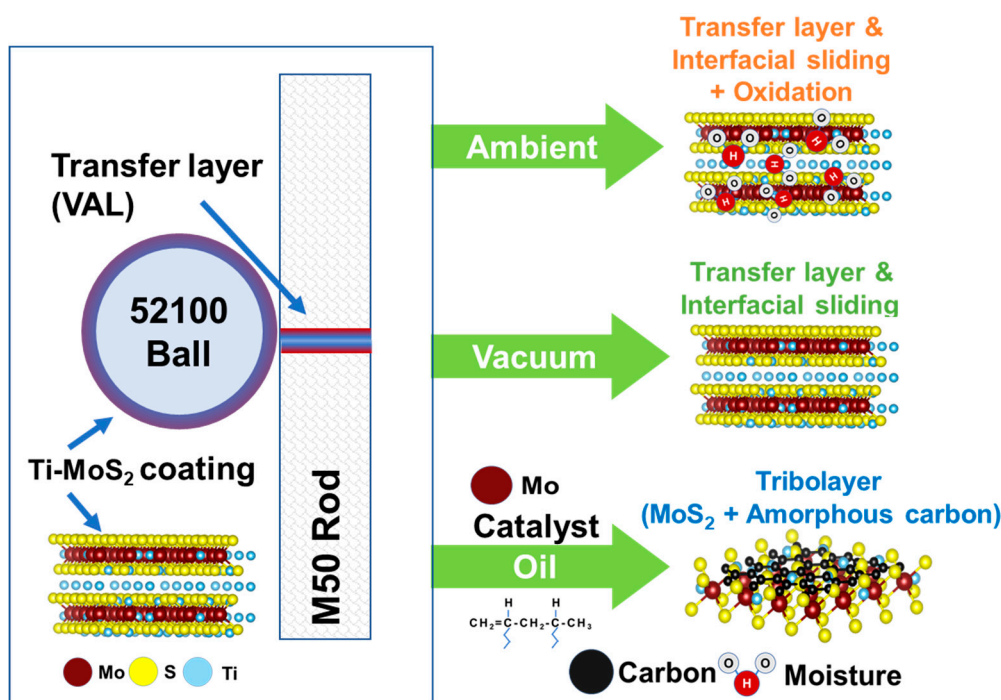


**Figure 5.** Schematic model for Ti-MoS<sub>2</sub>-coated balls tested against a M50 rod in ambient, vacuum, and oil environments with respective observed mechanisms.

Optical images of the wear track created in a M50 rod during the oil-lubricated test (Figure 4c) indicate no change in the surface topography of the rod, except for the presence of a tribofilm. Raman spectra of the tribofilm (Figure 4e) confirmed that the tribofilm consisted of crystalline MoS<sub>2</sub> (E<sup>1</sup><sub>2g</sub> and A<sup>1</sup><sub>g</sub> phonons) and amorphous carbon (D and G bands at 1382 and 1588 cm<sup>-1</sup> [40]). In our previous study [41], it was suggested that the formation of a hydrocarbon-rich tribofilm with MoS<sub>2</sub> precipitates was due to the synergistic effect of contact pressure and the catalytic behavior of Mo/MoS<sub>2</sub> in the presence of a hydrocarbon source (PAO ISO 10 oil).

Ti-MoS<sub>2</sub> deposited by the process used here has been shown to perform remarkably well in sliding contact [22,41,42]. Based on these new results, it can be concluded that the Ti-MoS<sub>2</sub> can also meet the VAL requirements in rolling contact and can be used to increase the operational lives of steel components that experience high cycle Hertz stresses in both rolling and sliding contacts.

#### 4. Conclusions

The rapidly widening range of conditions for mechanical systems and components provides new opportunities for the use of solid lubricants with and without oil lubrication. In this study, it was demonstrated that Ti (~16 at %)-containing MoS<sub>2</sub> coatings with a dense, featureless, and amorphous

microstructure improved rolling contact life of M50 bearing grade steels in ambient, vacuum, and oil-lubricated environments. Weibull analyses of  $L_{50}$  lifetimes of AISI 52100 steel balls coated with a Ti-MoS<sub>2</sub> coating paired with uncoated M50 steel rods were determined to be 3.7, 14.5, and 158.6 million cycles in ambient, vacuum, and oil-lubricated environments, respectively.

- In the ambient and vacuum tests, failures were determined to be associated with the onset of abrasive wear rather than fatigue or spalling.  $L_{50}$  lifetimes of tests performed in those environments were found to depend upon the amount of coating material available and its wear rate on the balls. That is, the Ti-MoS<sub>2</sub> functioned as a barrier to the onset of abrasive wear between the steel alloys until the coating was sufficiently worn away.
- Under oil-lubricated (boundary lubrication) conditions,  $L_{50}$  was found to depend on the durability and composition of tribofilms formed on the surfaces of the uncoated M50 rods. The tribofilms were found to be comprised of mixtures of MoS<sub>2</sub> crystallites and an amorphous hydrocarbon (a-C:H). The crystalline MoS<sub>2</sub> in the tribofilm obviously originated from the amorphous Ti-MoS<sub>2</sub> coating and likely underwent a thermodynamic phase transition as a result of the applied Hertz stress and frictional heating in the contact. The a-C:H in the tribofilm probably originated from a catalytic scission of the polyalphaolefin molecules caused by the d-band character of the Mo and/or Ti in the coating, similar to the results reported by Erdemir et al. [43].

Overall, Ti-MoS<sub>2</sub>-coated balls improved the  $L_{50}$  fatigue life of bearing steel by 34.91, 16.52, and 2.16 times in the respective ambient air, vacuum, and oil-lubricated environments compared to uncoated steel-steel material pairs. Results of this and previous studies indicate that the Ti-MoS<sub>2</sub> coating created from the process recipe used here can improve the tribological performance of mechanical components undergoing sliding or rolling contact that operate in ambient, vacuum, or oil-lubricated environments.

**Author Contributions:** G.L.D. conceptualized the idea; H.S. developed the coating; K.C.M. developed the methodology; H.S. and K.C.M. performed the experiments, and analyzed data; H.S. and K.C.M. contributed equally to the work; G.L.D. supervised the project and acquired funding; H.S., K.C.M., and G.L.D. contributed equally in manuscript preparation, editing and submission.

**Funding:** This research was funded by The Timken Company, North Canton, OH, USA.

**Acknowledgments:** The authors are thankful to Rich Fowler for his assistance in the development of vacuum tribometer and coating deposition. The authors wish to thank Ryan Evans from the Timken Company, Hamidreza Mohseni (now at Carbo Ceramics) and Thomas Scharf at UNT Center for Advanced Research and Technology (CART) for past contributions.

**Conflicts of Interest:** The authors declare no conflict of interest.

## References

1. Holmberg, K.; Erdemir, A. Influence of tribology on global energy consumption, costs and emissions. *Friction* **2017**, *5*, 263–284. [CrossRef]
2. Vazirisereshk, M.R.; Martini, A.; Strubbe, D.A.; Baykara, M.Z. Solid lubrication with MoS<sub>2</sub>: A review. *Lubricants* **2019**, *7*, 57. [CrossRef]
3. Scharf, T.W.; Prasad, S.V. Solid lubricants: A review. *J. Mater. Sci.* **2013**, *48*, 511–531. [CrossRef]
4. Sliney, H. Solid lubricant materials for high temperatures—A review. *Tribol. Int.* **1982**, *15*, 303–315. [CrossRef]
5. Hilton, M.R.; Bauer, R.; Fleischauer, P.D. Tribological performance and deformation of sputter-deposited MoS<sub>2</sub> solid lubricant films during sliding wear and indentation contact. *Thin Solid Films* **1990**, *188*, 219–236. [CrossRef]
6. Renevier, N.M.; Lobiondo, N.; Fox, V.C.; Teer, D.G.; Hampshire, J. Performance of MoS<sub>2</sub>/metal composite coatings used for dry machining and other industrial applications. *Surf. Coat. Technol.* **2000**, *123*, 84–91. [CrossRef]
7. Sliney, H. Solid Lubricants. Available online: <https://catalogue.nla.gov.au/Record/4036403> (accessed on 22 October 2019).
8. Zhao, X.; Perry, S.S. The Role of water in modifying friction within MoS<sub>2</sub> sliding interfaces. *ACS Appl. Mater. Interfaces* **2010**, *2*, 1444–1448. [CrossRef]

9. Curry, J.F.; Wilson, M.A.; Luftman, H.S.; Strandwitz, N.C.; Argibay, N.; Chandross, M.; Sidebottom, M.A.; Krick, B.A. Impact of microstructure on MoS<sub>2</sub> oxidation and friction. *ACS Appl. Mater. Interfaces* **2017**, *9*, 28019–28026. [[CrossRef](#)]
10. Stupp, B.C. Synergistic effects of metals co-sputtered with MoS<sub>2</sub>. *Thin Solid Films* **1981**, *84*, 257–266. [[CrossRef](#)]
11. Scharf, T.W.; Goeke, R.S.; Kotula, P.G.; Prasad, S.V. Synthesis of Au-MoS(2) nanocomposites: Thermal and friction-induced changes to the structure. *ACS Appl. Mater. Interfaces* **2013**, *5*, 11762–11767. [[CrossRef](#)]
12. Scharf, T.W.; Kotula, P.G.; Prasad, S.V. Friction and wear mechanisms in MoS<sub>2</sub>/Sb<sub>2</sub>O<sub>3</sub>/Au nanocomposite coatings. *Acta Mater.* **2010**, *58*, 4100–4109. [[CrossRef](#)]
13. Furlan, K.P.; de Mello, J.D.B.; Klein, A.N. Self-lubricating composites containing MoS<sub>2</sub>: A review. *Tribol. Int.* **2018**, *120*, 280–298. [[CrossRef](#)]
14. Zhang, X.; Luster, B.; Church, A.; Muratore, C.; Voevodin, A.A.; Kohli, P.; Aouadi, S.; Talapatra, S. Carbon nanotube-MoS<sub>2</sub> composites as solid lubricants. *ACS Appl. Mater. Interfaces* **2009**, *1*, 735–739. [[CrossRef](#)] [[PubMed](#)]
15. Mutyala, K.C.; Wu, Y.A.; Erdemir, A.; Sumant, A.V. Graphene–MoS<sub>2</sub> ensembles to reduce friction and wear in DLC-steel contacts. *Carbon* **2019**, *146*, 524–527. [[CrossRef](#)]
16. Zhang, M.; Chen, B.; Yang, J.; Zhang, H.; Zhang, Q.; Tang, H.; Li, C. MoS<sub>2</sub>/reduced graphene oxide hybrid structure and its tribological properties. *RSC Adv.* **2015**, *5*, 89682–89688. [[CrossRef](#)]
17. Grossiord, C.; Varlot, K.; Martin, J.; Le Mogne, T.; Esnouf, C.; Inoue, K. MoS<sub>2</sub> single sheet lubrication by molybdenum dithiocarbamate. *Tribol. Int.* **1998**, *31*, 737–743. [[CrossRef](#)]
18. Chhowalla, M.; Amaratunga, G.G.A.J. Thin films of fullerene-like MoS<sub>2</sub> nanoparticles with ultra-low friction and wear. *Nature* **2000**, *407*, 164–167. [[CrossRef](#)]
19. Liu, L.; Zhou, W. MoS<sub>2</sub> hollow microspheres used as a green lubricating additive for liquid paraffin. *Tribol. Int.* **2017**, *114*, 315–321. [[CrossRef](#)]
20. Rabaso, P.; Dassenoy, F.; Ville, F.; Diaby, M.; Vacher, B.; Le Mogne, T.; Belin, M.; Cavoret, J. An Investigation on the Reduced Ability of IF-MoS<sub>2</sub> nanoparticles to reduce friction and wear in the presence of dispersants. *Tribol. Lett.* **2014**, *55*, 503–516. [[CrossRef](#)]
21. Liu, Y.; Hu, K.; Hu, E.; Guo, J.; Han, C.; Hu, X. Double hollow MoS<sub>2</sub> nano-spheres: Synthesis, tribological properties, and functional conversion from lubrication to photocatalysis. *Appl. Surf. Sci.* **2017**, *392*, 1144–1152. [[CrossRef](#)]
22. Singh, H.; Mutyala, K.C.; Mohseni, H.; Scharf, T.W.; Evans, R.D.; Doll, G.L. Tribological performance and coating characteristics of sputter deposited Ti doped MoS<sub>2</sub> in rolling and sliding contact. *Tribol. Trans.* **2015**, *58*, 767–777. [[CrossRef](#)]
23. Zabinski, J.S.; Donley, M.S.; Walck, S.D.; Schneider, T.R.; Mcdevitt, N.T. The effects of dopants on the chemistry and tribology of sputter-deposited MoS<sub>2</sub> films. *Tribol. Trans.* **1995**, *38*, 894–904. [[CrossRef](#)]
24. Singh, H.; Mutyala, K.C.; Evans, R.D.; Doll, G.L. An investigation of material and tribological properties of Sb<sub>2</sub>O<sub>3</sub>/Au-doped MoS<sub>2</sub> solid lubricant films under sliding and rolling contact in different environments. *Surf. Coat. Technol.* **2015**, *284*, 281–289. [[CrossRef](#)]
25. Singh, H.; Mutyala, K.C.; Evans, R.D.; Doll, G.L. An atom probe tomography investigation of Ti–MoS<sub>2</sub> and MoS<sub>2</sub>–Sb<sub>2</sub>O<sub>3</sub>–Au films. *J. Mater. Res.* **2017**, *32*, 1710–1717. [[CrossRef](#)]
26. Vidakis, N.; Antoniadis, A.; Bilalis, N. The VDI 3198 indentation test evaluation of a reliable qualitative control for layered compounds. *J. Mater. Process. Technol.* **2003**, *143–144*, 481–485. [[CrossRef](#)]
27. Salloom, R.; Ayyagari, A.V.; Mukherjee, S. Nanoengineered hypereutectoid steel with superior hardness and wear resistance. *J. Mater. Eng. Perform.* **2019**, *28*, 2202–2211. [[CrossRef](#)]
28. Glover, D. A ball-rod rolling contact fatigue tester. In *Rolling Contact Fatigue Testing of Bearing Steels*; Hoo, J., Ed.; ASTM International: West Conshohocken, PA, USA, 1982; pp. 107–124.
29. Eichler, J.W.; Matthews, A.; Leyland, A.; Doll, G.L. The Influence of coatings on the oil-out performance of rolling bearings. *Surf. Coat. Technol.* **2007**, *202*, 1073–1077. [[CrossRef](#)]
30. Mutyala, K.C.; Singh, H.; Evans, R.D.; Doll, G.L. Effect of diamond-like carbon coatings on ball bearing performance in normal, oil-starved, and debris-damaged conditions. *Tribol. Trans.* **2016**, *59*, 1039–1047. [[CrossRef](#)]
31. Lubrecht, A.A.; Venner, C.H.; Colin, F. Film thickness calculation in elasto-hydrodynamic lubricated line and elliptical contacts: The Dowson, Higginson, Hamrock contribution. *Proc. Inst. Mech. Eng. Part. J. J. Eng. Tribol.* **2009**, *223*, 511–515. [[CrossRef](#)]

32. Kelly, P.J.; Arnell, R.D. Magnetron sputtering: A review of recent developments and applications. *Vacuum* **2000**, *56*, 159–172. [[CrossRef](#)]
33. Panjan, P.; Čekada, M.; Panjan, M.; Kek-Merl, D. Growth defects in PVD hard coatings. *Vacuum* **2009**, *84*, 209–214. [[CrossRef](#)]
34. Anders, A. A structure zone diagram including plasma-based deposition and ion etching. *China Surf. Eng.* **2016**, *29*, 1–6. [[CrossRef](#)]
35. Spalvins, T. Lubrication with sputtered MoS<sub>2</sub> films. *A S L E Trans.* **1971**, *14*, 267–274. [[CrossRef](#)]
36. Sadeghi, F.; Jalalahmadi, B.; Slack, T.S.; Raje, N.; Arakere, N.K. A review of rolling contact fatigue. *J. Tribol.* **2009**, *131*, 041403. [[CrossRef](#)]
37. Weibull, W. A statistical distribution function of wide applicability. *J. Appl. Mech.* **1951**, *18*, 293–297.
38. Danyluk, M.; Dhingra, A. Rolling contact fatigue using solid thin film lubrication. *Wear* **2012**, *274–275*, 368–376. [[CrossRef](#)]
39. Stoyanov, P.; Chromik, R.R.; Goldbaum, D.; Lince, J.R.; Zhang, X. Microtribological performance of Au–MoS<sub>2</sub> and Ti–MoS<sub>2</sub> coatings with varying contact pressure. *Tribol. Lett.* **2010**, *40*, 199–211. [[CrossRef](#)]
40. Ferrari, A.; Robertson, J. Resonant Raman spectroscopy of disordered, amorphous, and diamondlike carbon. *Phys. Rev. B* **2001**, *64*, 075414. [[CrossRef](#)]
41. Mutyala, K.C.; Singh, H.; Fouts, J.A.; Evans, R.D.; Doll, G.L. Influence of MoS<sub>2</sub> on the rolling contact performance of bearing steels in boundary lubrication: A different approach. *Tribol. Lett.* **2016**, *61*, 20. [[CrossRef](#)]
42. Paul, A.; Singh, H.; Mutyala, K.C.; Doll, G.L. An improved solid lubricant for bearings operating in space and terrestrial environments. In Proceedings of the 44th Aerospace Mechanisms Symposium, Cleveland, OH, USA, 16–18 May 2018; pp. 141–149.
43. Erdemir, A.; Ramirez, G.; Eryilmaz, O.L.; Narayanan, B.; Liao, Y.; Kamath, G.; Sankaranarayanan, S.K.R.S. Carbon-based tribofilms from lubricating oils. *Nature* **2016**, *536*, 67–71. [[CrossRef](#)]



© 2019 by the authors. Licensee MDPI, Basel, Switzerland. This article is an open access article distributed under the terms and conditions of the Creative Commons Attribution (CC BY) license (<http://creativecommons.org/licenses/by/4.0/>).